Effect of Train Shape on a Compression Wave Generated by a Train Moving into a Tunnel

Takanobu Ogawa* and Kozo Fujii**

* Shimizu Corporation,
Etchujima 3-4-17, Koto-ku,
Tokyo, 135 Japan

** The Institute of the Space and Astronautical Science,
Yoshinodai 3-1-1, Sagamihara
Kanagawa, 229 Japan

Abstract

An axisymmetric flow induced by a train moving into a tunnel is numerically simulated. The effect of train shape on wavefront of a compression wave created by a train is investigated parametrically using several model trains having the same nose shape but different blockage. The zonal method combined with the Fortified Solution Algorithm (FSA) is employed as a numerical algorithm to solve this moving body problem. The computational result is compared with the experimental data. Good agreement is obtained, which justifies the present computational approach. The compression waves created by the model trains are compared and the result shows that the pressure gradient of the wavefront of the compression wave becomes small in the case of small blockage even though the nose shape is same. The wavefront is not determined solely by the cross-sectional area distribution of the train nose.

1 INTRODUCTION

High speed trains are being developed in recent years. Speed of the trains is becoming more than Mach number 0.2. At this high speed, compressibility of air should be considered and substantial aerodynamic problems may occur particularly under tunnel entry. When a high speed train moves into a tunnel, the pressure inside the tunnel increases and a compression wave is generated in front of the train and it propagates towards the exit of the tunnel. When going out through the exit, the compression wave becomes a pulse-like wave and it propagates around the exit. This pulse-like wave may sometimes cause a booming noise and is called a Micro-Pressure wave[1]. The strength of the Micro-Pressure wave is essentially proportional to $U_t{}^3$, where U_t is the speed of the train[2]. Thus, it is important not to increase the strength of the Micro-Pressure wave by finding and changing the other effective parameters for developing a high speed train. Ozawa[1] studied the relation of the strength of the Micro-Pressure wave and the compression wave at an exit of the tunnel with the linear acoustic theory. According to the result, the strength of a Micro-Pressure wave is proportional to the pressure gradient of the wavefront of the compression wave at the exit and it is important to make the wavefront of the compression wave mild to alleviate the Micro-Pressure wave.

It may be possible to smooth the wavefront of the compression wave by modifying train shapes. However, the relation between the train shape and the wavefront has not been clarified so far. In this paper, the axisymmetric flow field where model trains having the same cross sectional area distribution of the train nose but the different blockage, i.e., the ratio of the cross sectional area of the train to that of the tunnel move into a tunnel is numerically simulated for the investigation of the effect of the blockage on the wavefront of the compression wave in case of the same shape of the train nose. The numerical result is validated with the experimental data. The wavefront of the compression wave created by the model trains are compared and the effect of the train shape on the wavefront of the compression wave is discussed.

2 NUMERICAL METHOD

2.1 The Governing Equations and Numerical Scheme

The governing equations are the axisymmetric compressible Euler equations written in the generalized coordinate system,

$$\partial_t \hat{Q} + \partial_\xi \hat{E} + \partial_\eta \hat{F} + \hat{G} = 0 \tag{1}$$

where

$$\hat{Q} = \frac{r}{J}\begin{bmatrix} \rho \\ \rho u \\ \rho v \\ e \end{bmatrix}, \hat{E} = \frac{r}{J}\begin{bmatrix} \rho U \\ \rho u U + \xi_x p \\ \rho v U + \xi_y p \\ (e+p)U - \xi_t \end{bmatrix}, \hat{F} = \frac{r}{J}\begin{bmatrix} \rho V \\ \rho u V + \eta_x p \\ \rho v V + \eta_y p \\ (e+p)V - \eta_t \end{bmatrix}, \hat{G} = \frac{r}{J}\begin{bmatrix} 0 \\ 0 \\ -p/r \\ 0 \end{bmatrix} \tag{2}$$

U, V are the contravariant velocity components and J is the transformation Jacobian. r denotes the distance from the symmetry axis. Pressure p is related to density ρ, the total energy e and the velocity vector components u, v for an ideal gas by

$$p = (\gamma - 1)\left\{ e - \frac{1}{2}\rho(u^2 + v^2) \right\} \tag{3}$$

where γ is the ratio of specific heats.

The convective terms are discretized using Roe's flux difference splitting[4]. The primitive-variable extrapolation of MUSCL approach[5] is used to establish second-order accuracy.

2.2 Fortified Solution Algorithm (FSA)

The flow field where a train moves into a tunnel contains the relative motion of the boundary. In this paper, the zonal method is used to solve the moving-boundary problem. Interface algorithm is essential to the efficiency and accuracy of the zonal method. The Fortified Solution Algorithm(FSA)[6] is used to transfer the physical data from one zone to another. When the FSA is applied to the axisymmetric Euler equations, the governing equations (1) are modified as follows

$$\partial_t \hat{Q} + \partial_\xi \hat{E} + \partial_\eta \hat{F} + \hat{G} = \chi(\hat{Q}_f - \hat{Q}) \tag{4}$$

The source terms are added to the right hand side of the original Euler equations, Eq. (1). χ is a switching parameter and is set to be a sufficiently large value in the interface region where zones are overlapped each other. When χ is large, Eq. (4) forces $\hat{Q}_f = \hat{Q}$ and $\hat{Q}$ is replaced with $\hat{Q}_f$. The $\hat{Q}_f$ is set to the solution of the other zone in the interface region. Equations (4) become the original Euler equations outside the interface region where $\chi = 0$. There is no special and troublesome treatment on boundaries to transfer the physical data. Only needed is to set χ to be appropriate values in the FSA approach. Implementing the FSA to the existing codes is also straightforward. Two-stage explicit time integration is used in this paper. The final form of the time integration becomes,

$$\begin{aligned} \hat{Q}^* &= \hat{Q}^n + R(\hat{Q}^n) && (1st\ step) \\ \hat{Q}^{n+1} &= \hat{Q}^n + \tfrac{1}{2}\{R(\hat{Q}^n) + R(\hat{Q}^*)\} + \tfrac{h\chi}{1+h\chi}(\hat{Q}_f - \hat{Q}^n) && (2nd\ step) \end{aligned} \tag{5}$$

where,

$$R(\hat{Q}^n) = \frac{h}{1+h\chi}(\partial_\xi \hat{E} + \partial_\eta \hat{F} + \hat{G})^n, h = \Delta t \tag{6}$$

2.3 Flow Field and Grid Configuration

The flow field is schematically illustrated in Fig. 1, which simulates the experiment by Maeda et. al.[3]. The exit of the tunnel is not attached in the computation, since generation of a compression wave at

an entrance of a tunnel is of our main interest. The diameter of the tunnel is taken as a reference length and the tunnel is 50.0 long. The train is located at x=-3.0 at the beginning and moves impulsively in the positive X-direction. The flow field is divided into five zones for the present zonal method. The composite flow field and its grid distributions are shown in Fig. 2. One of the zones is prepared to resolve the flow field around the train (Fig. 2(b)). It moves at the train speed and is overlaid on the base grids. The base grids are composed of the entrance zone and the tunnel zone. Their grid points are 203x41 and 528x21, respectively (Fig. 2(a)). Since the grid points of the train and the tunnel zone do not coincide in the overlap region, the physical data to be transferred should be determined by the linear interpolation with the surrounding points in the other zone. Thus, the surrounding points should be searched in every time step and it would take about 20% of the total computer time, although the flow field could be solved with these three zones. To reduce this computer overhead, an intermediate zone that moves at the same speed as the train is overlaid on the train zone. Now, the transfer of the physical data between the train and tunnel zone is carried out through the intermediate zone. It is not necessary to search the surrounding grid points at every time step between the train and the intermediate zone, since this two zones move at the same speed and there is no relative motion between them. Furthermore, the intermediate zone and the tunnel zone are both rectangular grid, thus the one dimensional searching is only necessary at every time step and it takes much less computer time than two dimensional searching. The grid points of the intermediate zone are 131x41 and therefore the grid resolution is also improved. In addition, the collar zone is prepared to remove a singular point at the corner of the tunnel entrance. The number of grid points in this zone is 51x21. These two additional zones are shown in Fig. 2(b).

The four model trains, called type 1, 2, 3 and 4 are used. They are shown in Fig. 3. The blockage ratios, i.e., the ratio of the cross sectional area of the train to that of the tunnel, of type 1, 2, 3 and 4 are 0.250, 0.116, 0.060 and 0.030, respectively. All the train nose has same parabolic nose shape. Figure 4 shows the cross sectional area distribution. The cross sectional area of the train nose varies linearly and the maximum gradient of the cross sectional area is the same in all the cases. The speed of all trains is 0.188 and the trains reach at the tunnel entrance at t=0.0.

3 RESULTS

Time sequence of the pressure contour plots of type 2 are presented in Fig. 5 to illustrate the typical time sequence of the flow field. At t=-1.96, the train is getting closer to the tunnel and the pressure inside the tunnel is beginning to increase. When the train enters the tunnel (t=1.04, and 2.04). The pressure in the tunnel increases and a compression wave is being created in front of the train. The compression wave is observed as vertical contour lines aligned in the spanwise direction in the tunnel and is found to be a plane wave. At t=3.04, the compression wave propagates towards the exit faster than the train.

Pressure distributions along the tunnel wall at several time steps are plotted in Fig. 6. The pressure peaks indicated by the arrows in the figure are the compression wave and the expansion wave generated at the nose and the tail of the train when the train moves impulsively at t=0.0 and these waves are out of interest in this paper. The pressure distribution at t=-0.96 indicates that the pressure inside the tunnel increases before the train enters the tunnel. After the train enters the tunnel, the pressure inside the tunnel continues to increase and the compression wave develops, as is seen from the pressure distribution at t=4.04 and 9.04 in the figure. Then the pressure increase stops, and the compression wave is fully developed and propagates towards the tunnel exit at almost the speed of sound.

Figure 7 shows the velocity vector plots at the entrance at t=7.04. The flow is induced from the inside of the tunnel towards the outside since the pressure is high in front of the train. However, as shown in Fig. 6, the pressure at the side of the train almost keeps the atmospheric pressure while the train is moving into the tunnel. Thus, the pressure decrease due to the outflow can be negligible.

The time history of the pressure inside the tunnel at x=6.8 for type 2 is compared with the experimental data[3] in Fig. 8. The peaks found at t=-0.0025 sec and 0.0005 sec in the computed pressure history are the pressure waves generated by the impulsive start and do not seem to affect the compression wave itself. The plot shows good agreement between the computational results and the experimental data.

The time history of the pressure inside the tunnel at x=6.8 for all the cases is plotted in Fig. 9. They

are drawn as solid lines and compared with the one-dimensional flow model[7] plotted as dashed lines. In the one-dimensional flow model, the compression of the fluid inside the tunnel is expressed as the change of the cross sectional area of the tunnel in time due to the tunnel entry of the train. The maximum pressure increases inside the tunnel of the one-dimensional flow model is almost the same as that of the present computation. However, there are discrepancies about the wavefront of the compression wave between the two method. Firstly, the pressure inside the tunnel begins to increase before the train enters the tunnel in the axisymmetric computation, while the pressure increase begins when the train reaches at the tunnel entrance in the one-dimensional model. Secondary, the pressure gradient of the wavefront of the compression wave becomes smaller as the blockage ratio becomes small in the axisymmetric computation. On the other hand, one-dimensional model shows the same wavefront of the compression wave until the train nose completely enters the tunnel. The wavefront of the compression wave is not determined only by the cross-sectional are distribution of the train nose but also by the blockage ratio and one-dimensional model, in which the pressure increase inside the tunnel is caused by the decrease of the cross sectional area of the tunnel due to the tunnel entry of the train, fails to predict the wavefront of the compression wave. Accurate prediction of wavefront of the compression wave is very important because the strength of the booming noise propagating from the exit depends on the time derivative of the compression wave. The present result indicates that the increased pressure level can be predicted by the one-dimensional method but multi-dimensional model is necessary for the evaluation of the wavefront.

4 SUMMARY

The flow field induced by a train moving into a tunnel is numerically simulated under the assumption of axisymmetric flows. The effect of train shape on the wavefront of a compression wave created by a train is investigated parametrically using several model trains having the same cross sectional area distribution of the train nose but different blockage ratio. The present approach is validated by the good agreement with the experimental data. The result shows that the wavefront of the compression wave becomes smaller when the blockage becomes small even when the nose shape is same. This indicates that the wavefront of the compression wave is not determined solely by the cross sectional area distribution of the train nose. Therefore, the wavefront of the compression wave cannot be predicted by a one-dimensional flow model and multi-dimensional flow model is required for the evaluation of the booming noise.

References

[1] Ozawa, S. : "Studies of Micro-pressure Wave Radiated from a Tunnel Exit," Railway Technical Research Report, No.1121, Jul., 1979, (In Japanese)

[2] Yamamoto, A. : "Aerodynamics of Train and Tunnel," Railway Technical Research Report, No.1230, Mar., 1983, (In Japanese)

[3] Maeda, T. :"Effect of Shape of Train Nose on Compression Wave Generated by Train Entering Tunnel, " The International Conference on Speedup Technology for Railway and Maglev Vehicles, pp. 315-319, 1993

[4] Roe, P. :"Approximate Riemann Solvers, Parameter Vectors, and Difference Schemes," Journal of Computational Physics, 43, pp. 357-372, 1981

[5] Van Leer, B., Thomas, J. L., Roe, P. L., and Newsome, R. W. :"A Comparison of Numerical Flux Formulas for the Euler and Navier-Stokes Equations," AIAA paper 87-1104CP, 1987

[6] Fujii, K. :"Unified Zonal Method Based on the Fortified Navier-Stokes Concept," AIAA-91-1558, 1991

[7] Watanabe, R., Higashino, F. and Fujii, K. :"One Dimensional Analysis of a Compression Wave Induced by a Train Moving into a Tunnel," 7th Symposium of Computational Fluid Dynamics, 1993, (In Japanese)

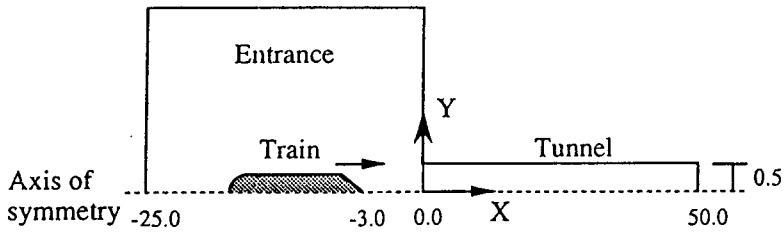

Fig. 1 : Flow field

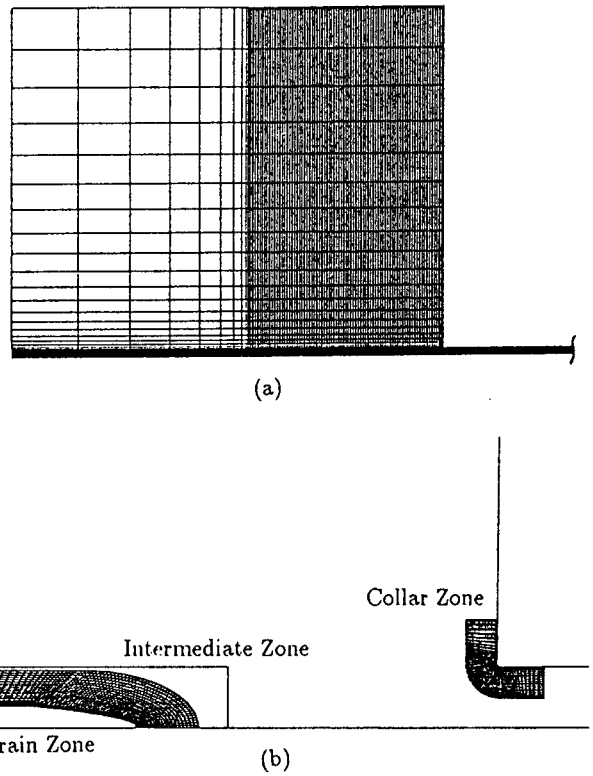

Fig. 2 : Grid distribution

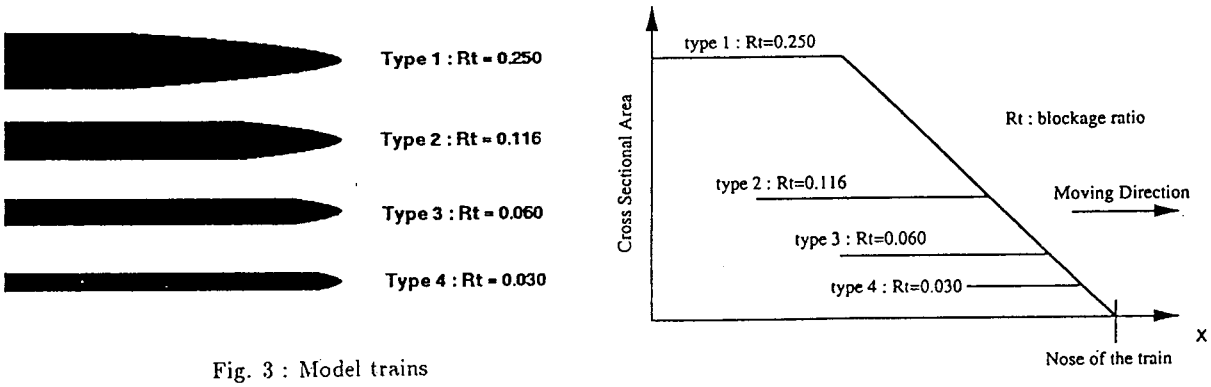

Fig. 3 : Model trains

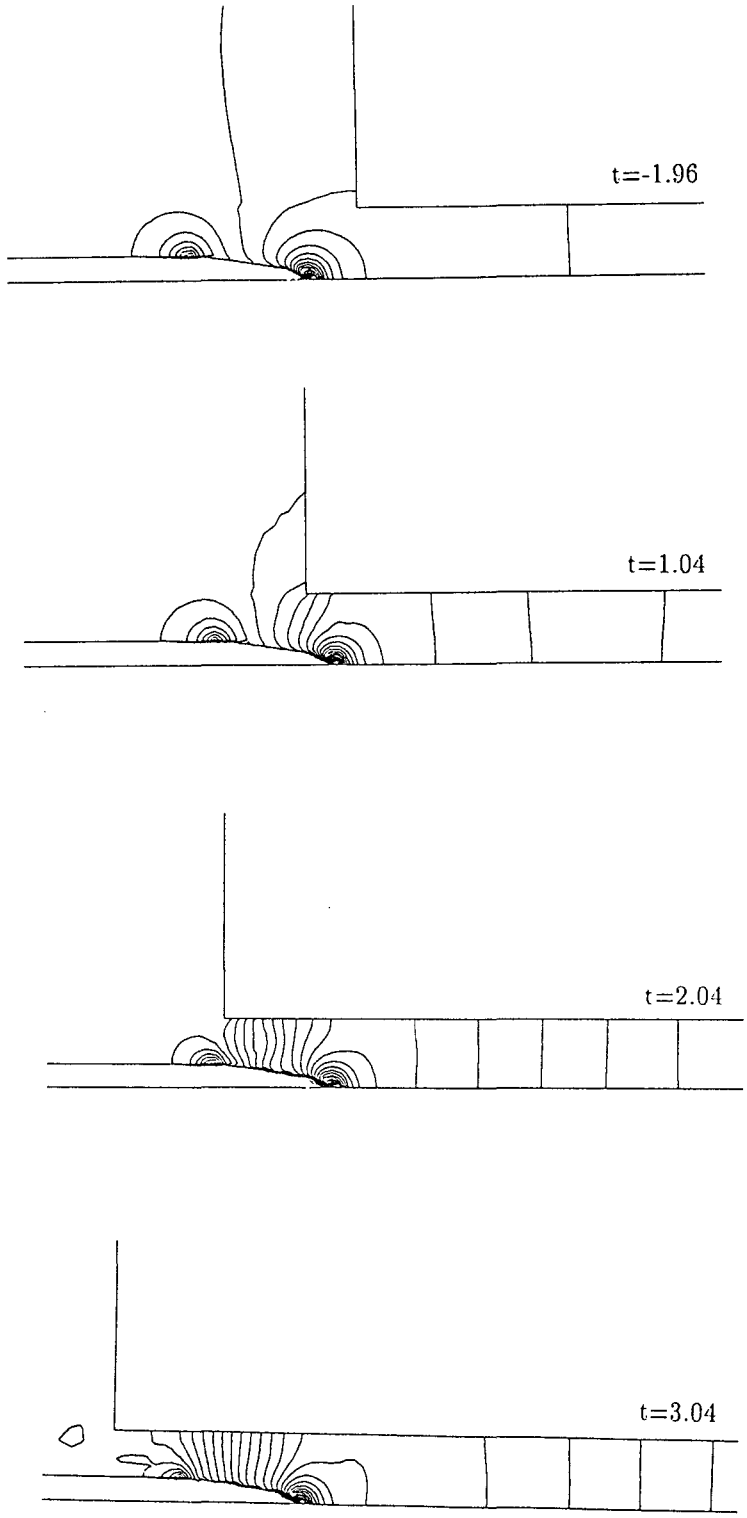

Fig. 5 : Pressure contour plots of type 2

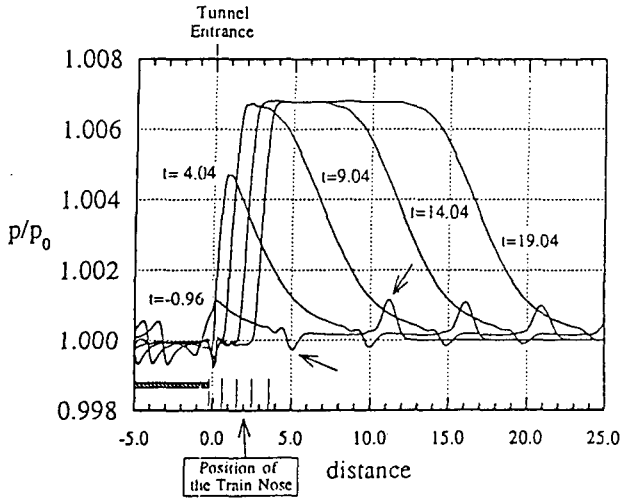

Fig. 6 : Time sequence of the pressure distributions at the tunnel wall (Type 2)

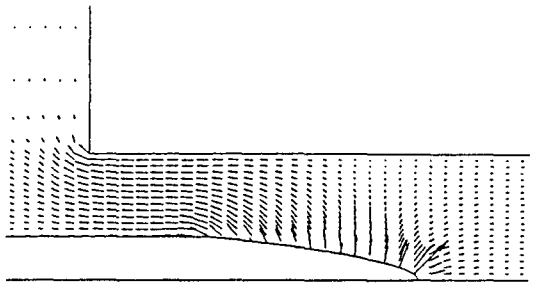

Fig. 7 : Velocity vector plots at the entrance at t=7.04 (Type 2)

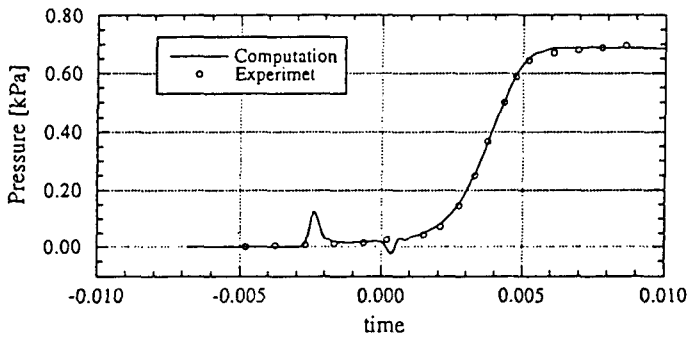

Fig. 8 : Pressure history inside the tunnel, the experimental data by Maeda et.al.[3)]

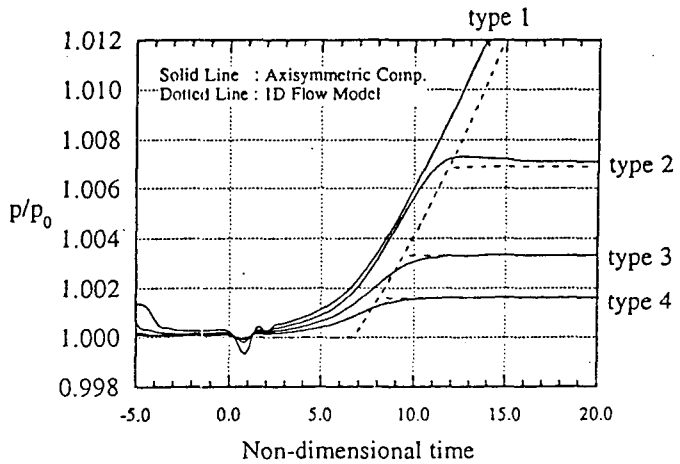

Fig. 9 : Pressure history inside the tunnel